COMMUNICATION

Chemical Vapor Deposition Growth of Linked Carbon Monolayers with Acetylenic Scaffoldings on Silver Foil

Rong Liu, Xin Gao, Jingyuan Zhou, Hua Xu, Zhenzhu Li, Shuqing Zhang, Ziqian Xie, Jin Zhang, and Zhongfan Liu**

After the successful synthesis of fullerene,[1] carbon nanotube,[2] and graphene,[3] new synthetic carbon allotropes with novel structure and outstanding properties are inspired to be explored, such as graphyne[4] and graphdiyne.[5] Graphdiyne, a monolayer of sp- and sp^2-bonded carbon atoms, is a new form of two-dimensional (2D) carbon material like graphene. It contains diacetylenic linkages between carbon hexagons with extended π-conjugation structure. Graphdiyne is predicted to exhibit impressive properties such as high third-order nonlinear optical susceptibility,[6] extreme hardness,[7] uniformly distributed pores, low thermal conductivity,[8] and high charge carrier mobility,[9,10] making it a good candidate for applications in electronic devices, energy storage,[11] gas separation,[12] photocatalysis,[13] nonlinear optics,[6] etc. Many experimental efforts have been made on synthesizing and characterizing this material since the first report on the preparation of a 1 μm-thick graphdiyne film.[14] The classic synthetic route is the oxidative coupling of hexaethynylbenzene (HEB) under the catalysis of copper ions in organic solution. In this approach, a copper foil is usually used as substrate for both supplying catalytic ions and supporting the growth of graphdiyne film. With this method, graphdiyne of various thickness[14,15] and morphologies[16] have been achieved, while different kinds of applications based on such materials have been demonstrated.[13,17–19] However, a solution method is limited to the lack of controllability in thickness, morphology, and structure of the materials because of the random distribution of catalytic copper ions in solution. So far, monolayer graphdiyne is still not available, which hinders the fundamental studies of the intrinsic properties. Therefore, it is important to develop a synthetic route for monolayer graphdiyne with well-defined structure over large area.

R. Liu, X. Gao, J. Y. Zhou, Prof. H. Xu, Z. Z. Li, S. Q. Zhang, Z. Q. Xie, Prof. J. Zhang, Prof. Z. F. Liu
Center for Nanochemistry
Beijing Science and Engineering Center for Nanocarbons
Beijing National Laboratory for Molecular Sciences
College of Chemistry and Molecular Engineering
Peking University
Beijing 100871, P. R. China
E-mail: jinzhang@pku.edu.cn; zfliu@pku.edu.cn
R. Liu, J. Y. Zhou, Z. Z. Li, S. Q. Zhang
Academy for Advanced Interdisciplinary Studies
Peking University
Beijing 100871, P. R. China
Prof. H. Xu
School of Materials Science and Engineering
Shaanxi Normal University
Xi'an 710119, P. R. China

DOI: 10.1002/adma.201604665

In recent years, on-surface covalent synthesis, by which nanostructures are constructed on metal surfaces through covalent bonding of organic precursors, has been recognized as a promising strategy for the fabrication of new 2D materials. This approach has already been applied to the synthesis of various 2D networks with atomic precision.[20–22] In the process of on-surface synthesis, the growth of materials is self-limited since there is no catalyst to activate reaction and promote growth once the metal surface is fully covered. Such a synthetic approach could be realized through the chemical vapor deposition (CVD) process which generally provides a substrate surface for the reaction of deposited precursors transferred by a carrier gas. Therefore, the CVD process might be a proper approach for the growth of monolayer graphdiyne. To construct the structure of graphdiyne, a surface-assisted homocoupling reaction of terminal alkynes on a metal surface is required. Corresponding research in ultrahigh vacuum (UHV) system have already been demonstrated.[23,24] Though a Glaser coupling reaction in solution is mediated by copper complexes, the surface-assisted coupling reaction is not efficient on a Cu substrate.[25,26] Statistical analysis results show that a Ag substrate is the most efficient substrate for a surface-assisted coupling reaction which provides the lowest proportion of side reactions compared to Au and Cu substrates.[26,27] In addition, previous work also has found that the metal substrate would influence the morphologies of nanostructures through adsorption energies, diffusion barriers, and lateral interactions of molecular precursors. The surface on which molecule diffusion prevails over intermolecular coupling is better for the construction of regular 2D network.[28] In this regard, a Ag substrate is suitable for conducting on-surface homocoupling of terminal alkynes and therefore is selected as catalytic substrate in our system.

Herein, we demonstrated the synthesis of a monolayer carbon network with acetylenic scaffoldings, graphdiyne analogs, through a CVD process by using HEB, an arylalkyne compound, as a precursor. The uniform monolayer structure was investigated by optical microscope (OM) and atomic force microscopy (AFM) characterization, which indicated that the on-surface process governed the growth of the carbon film. The upshift of Raman peak corresponding to arylalkyne from 2106 to 2180 cm^{-1} exhibited the successful conversion of the HEB monomer to the linked network through the surface-assisted homocoupling reaction of terminal alkynes. The electrical transport measurements showed that the as-grown film displayed a semiconducting feature with conductivity of 6.72 S cm^{-1}. Moreover, the film was also considered as a good substrate for suppressing fluorescence and enhancing Raman signals of adsorbed molecules.

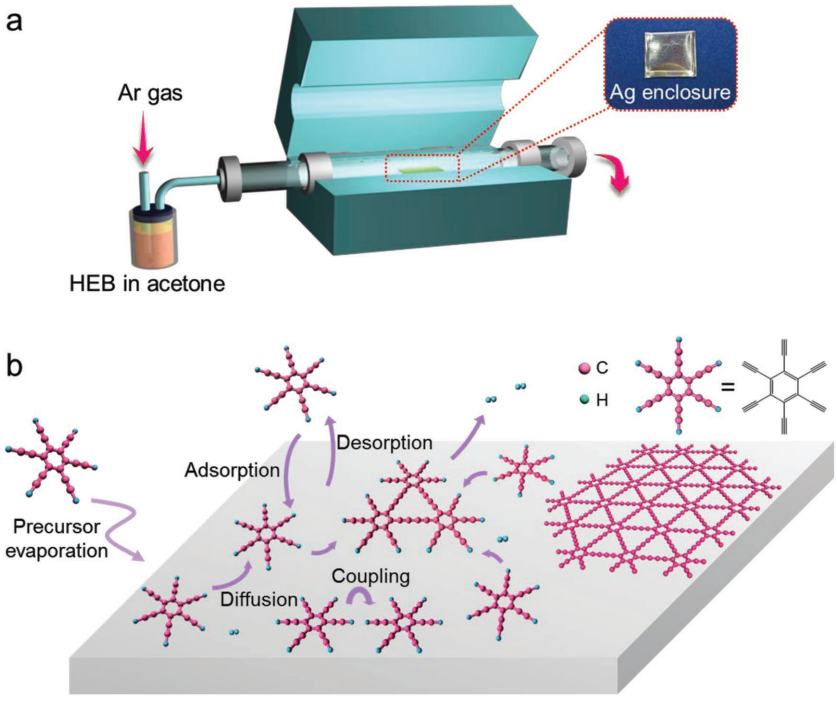

Figure 1. a) Experimental setup of the CVD system for the growth of linked carbon monolayer on silver surface using HEB as precursor. b) Schematic view of the surface growth process.

As an appealing and versatile synthetic strategy, the CVD method has already been extensively used for the growth of various 2D materials. A typical CVD growth process is usually carried out at high temperature which helps precursors adsorbed on the substrate surface decompose into active species as a growth source. Compared with graphene growth, the CVD growth process of graphdiyne is quite different. As graphdiyne consists of two kinds of hybridized carbon atoms, the building blocks of graphdiyne are molecules containing phenyl and alkynyl groups while that of graphene are sp^2-hybridized carbon atoms obtained from the thermal decomposition of precursors. The growth of graphdiyne is realized by the covalent bonding between precursor molecules with terminal alkynes, so it is important to maintain the molecular skeleton structure during the growth process. High temperature will damage the molecular skeleton structure of precursor. Therefore, a low temperature is needed for the CVD growth of graphdiyne.

The CVD system employed in this work is depicted in **Figure 1**a. A silver-foil enclosure method described in a previous study[29] was used here in which the deposition rate of precursor could be controlled easily. It also has been found that the inner surface of the silver enclosure is much smoother than the outer surface after annealing due to less loss of silver by thermal evaporation.[30] The rough surface would hinder the diffusion of monomer precursors on it, which is adverse to the formation of regular 2D networks. So a silver-foil enclosure was used and the linked carbon film was obtained from the inside surface. The precursor HEB was put upstream and transported by carrier gas to the silver surface held at low temperature. We dissolved HEB in acetone because HEB would polymerize into uncertain insoluble matter by heating easily due to its high chemical activity. The growth temperature was decided according to the thermogravimetric analysis-differential scanning calorimetry (TGA-DSC) of hexakis[(trimethylsilyl) ethynyl]benzene (Figure S2, Supporting Information). From the TGA-DSC result we concluded that the molecule was thermally stable from room temperature to 200 °C as there was no obvious mass change or heat flux peak within this temperature zone. Moreover, referring to the studies on covalent homocoupling of terminal alkynes on metal surface in UHV system,[23,24,27] we chose 150 °C as the growth temperature. Figure 1b schematically illustrates the idealized growth process of graphdiyne. On thermal activation and substrate catalysis, covalent C—C linkage of alkynyl groups between two adsorbed monomers formed with the cleavage of C_{sp}—H bond. After the growth process, a continuous film was obtained on the surface of Ag foil.

The SEM image of the linked carbon film on Ag foil after CVD growth is shown in Figure S3a in the Supporting Information. The Ag grain boundaries are evidently visible (pointed out by yellow arrows).[31,32] The as-grown film can be easily transferred from the growth substrate onto arbitrary substrates using a poly(methyl methacrylate) (PMMA)-mediated technique for subsequently exploring the properties and applications. **Figure 2**a shows the OM image of the as-grown film transferred onto a SiO_2 (300 nm)/Si substrate. We can see that the color of the film is quite different from that of the bare substrate, and the film shows good uniformity and continuity. The SEM image of the film on the SiO_2/Si substrate (Figure S3b, Supporting Information) shows the film has large area uniformity without any cracks. The red arrows point out the wrinkles caused by the transfer process, indicating that the as-grown film is continuous. AFM characterization shows a height of 0.6 nm (Figure 2b), revealing the monolayer nature of the film. Transmission electron microscopy (TEM) was used to analyze the morphology and microstructure of the film. Figure 2c is the low-resolution TEM image of the film suspended on TEM copper grids, which further verifies the successful synthesis of continuous film. The inset is the corresponding selected area electron diffraction (SAED) pattern indicating the noncrystalline nature of the film, which means that the structure of the film shows no significant in-plane order over relatively large area. One possible reason for the formation of the unordered structure may be the influence of side reactions especially the addition reaction between two adjacent terminal alkynes occurred during the on-surface synthesis process.[33] Smarter design of the catalytic environment such as surface templating[24] and optimal molecular design[27] may be needed to construct well-ordered molecular nanostructures.

Raman spectrum and UV–visible (UV–vis) absorption spectrum provided useful methods to monitor the conversion from monomers to the linked carbon film. Two typical Raman peaks

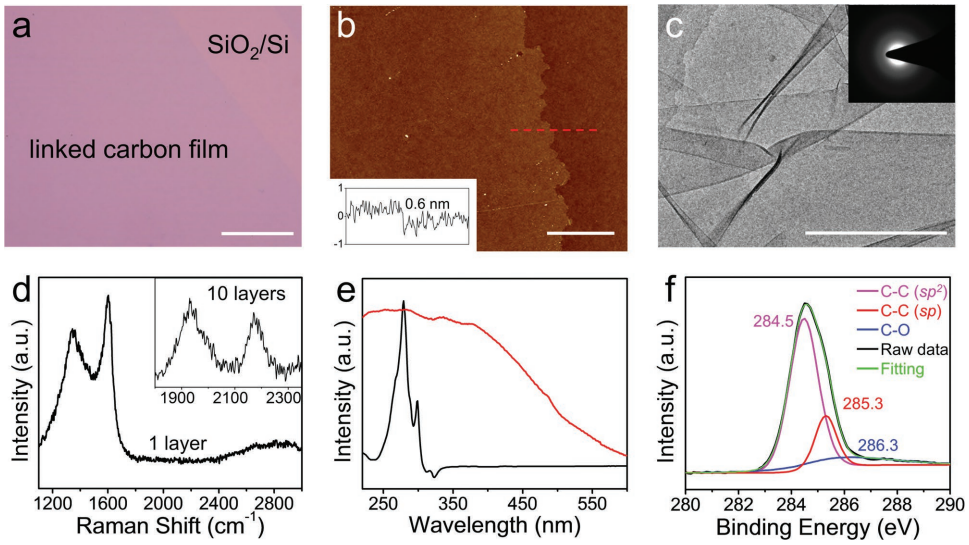

Figure 2. Morphological and spectroscopic characterization of linked carbon film grown with HEB. a) OM image of the as-grown film transferred on a SiO_2/Si substrate. b) AFM image of the film transferred on SiO_2/Si. Inset: height profile along the dashed red line. c) Low-resolution TEM image of the film suspended on TEM copper grids. Inset: corresponding SAED pattern. d) Raman spectrum of the as-grown film transferred onto SiO_2/Si. Inset: Raman spectrum of 10-layer transferred film on silver substrate. e) Absorption spectra of HEB in THF (black line) and the transferred film (red line) on quartz. f) C 1s XPS spectrum of the as-grown film. Scale bars, 50 µm in (a), 1 µm in (b) and (c).

corresponding to the breathing vibration of aromatic ring centered at 1358 cm^{-1} (D band) and the first order scattering of the E_{2g} mode for in-plane stretching vibration of sp^2 atoms centered at 1595 cm^{-1} (G band) were obtained (Figure 2d). We did not observe any peaks from alkynyl group in the as-grown film due to the weaker signal of alkynyl group than the detection limit of the instrument. However, when we overlaid the film layer by layer for ten times on a silver surface which can be regarded as a substrate for Raman enhancement,[34,35] the peak at 2180 cm^{-1} which is attributed to the C≡C stretching mode in conjugated diyne links[16,36] was clearly observed (Figure S4a, Supporting Information). This peak is blue shifted compared to the peak from HEB monomer centered at 2106 cm^{-1} corresponding to the C≡C stretching mode in terminal arylalkynes (Figure S5, Supporting Information). The blue shift quantity is consistent with previous experimental literature results.[16] This change of Raman signals indicates the conversion of HEB monomers to the corresponding linked film. However, we have not found any explicit theoretical assignments to 1940 cm^{-1}, which was also observed in previous reports on the synthesis of graphdiyne.[14,16] The uniformity of as-grown film was further confirmed with Raman mapping data generated from 2080 to 2300 cm^{-1} which shows uniform Raman intensities distribution over large area (Figure S4b, Supporting Information). UV–vis absorption spectrum of the film transferred to a UV grade quartz slide possesses a broad new peak around 350 nm compared to the monomer in tetrahydrofuran (THF) (Figure 2e), which is attributed to the increased delocalization of electron in extended π-conjugated system.[36] The corresponding optical transmission spectrum in Figure S6 in the Supporting Information shows that the film is almost completely transparent in the UV–vis region. And the optical transmittance increases up to 100% with the increase of wavelength.

X-ray photoelectron spectroscopy (XPS) was performed to determine the elemental composition and chemical state of the elements existing within the film. Full and C 1s XPS spectra are shown in Figure S7 in the Supporting Information and Figure 2f, respectively. In C 1s region, the result shows that there is one broad peak at the binding energy of 284.5 eV, which results from the overlapping of signals of several carbon species with close binding energies. The experimental curve is fitted with three subpeaks at 284.5, 285.3, and 286.3 eV assigned to the orbital of C=C (sp^2), C≡C (sp), and C—O, respectively. The small peak of C—O species is mainly due to the physisorption of oxygen-containing molecule from air or some slight oxidation of terminal alkynes within the film.

Furthermore, field-effect transistors (FETs) were fabricated to probe the charge transport characteristics of the linked carbon film. The schematic depiction of the FET device is shown in **Figure 3**a. The conductivity of the film originated from the extensive conjugated sp^2- and sp-carbon networks. Typical I–V_{ds} characteristics of the film are shown in Figure 3b. The linear and symmetric profile suggests the ohmic contacts with electrodes. The measured resistance of the film is 0.31 MΩ and the corresponding conductivity is 6.72 S cm^{-1}. Figure 3c shows the transfer characteristics of a typical device. The conductance decreases as the gate voltage (V_{gate}) sweeps from negative (–50 V) to positive (50 V) value, which suggests a p-type semiconducting feature. However, the channel does not switch from "on" state to complete "off" state by the modulation of gate voltage. To investigate the electronic uniformity and the overall quality of as-grown film, we fabricated an array of devices with the same configuration (Figure S8a, Supporting Information). We measured I–V curves of these devices one by one under the same conditions, and gave a spatial distribution map of calculated electrical resistance (Figure 3d). The corresponding statistical analysis of electrical resistance distribution is shown

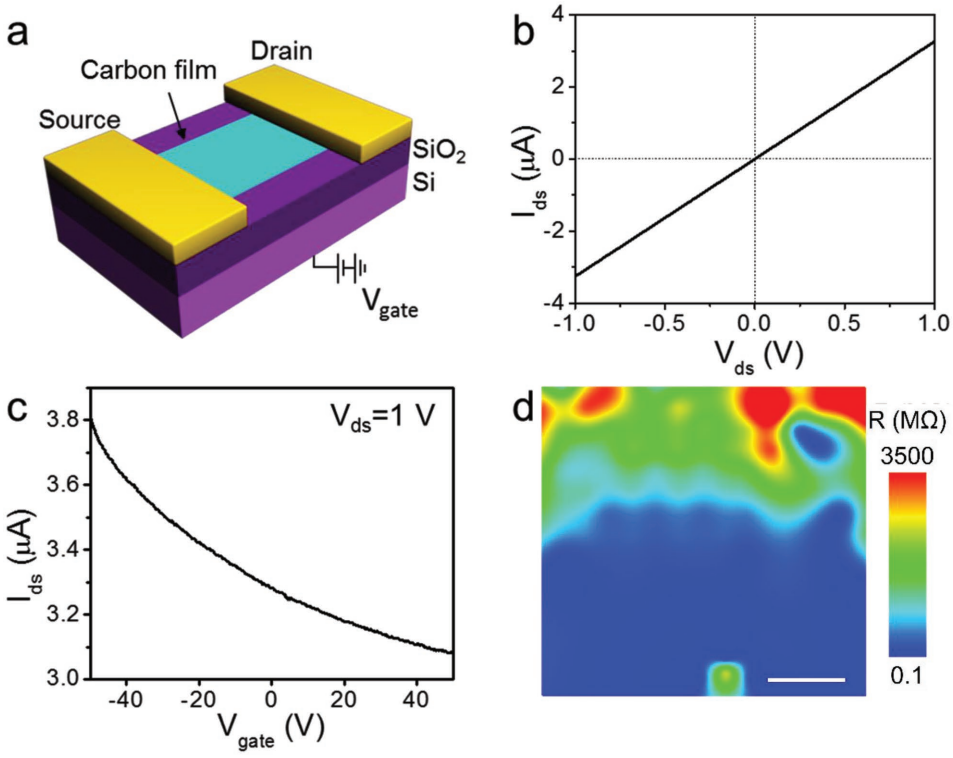

Figure 3. Electrical properties of the linked carbon film grown with HEB. a) Schematic illustration of a two-terminal back-gated FET device fabricated on the film. b) *I–V* characteristic of the film. c) Transport characteristic curve of the device at V_{ds} = 1 V. d) 2D color plot of the electrical resistance of a 112-FET-device array made on the film. Scale bar, 100 μm.

in Figure S8b in the Supporting Information. The result shows that in some areas (colored in blue), the as-grown film exhibits uniform distribution of resistance with low value indicating the good quality of the film. There are also some areas which show much larger variation. The differences in electrical resistance reveal the differences in the quality of the film which could result from the local perturbation of gas flow or the nonuniformity of substrate surface.

In order to demonstrate the universality and further explore the possibility to grow new 2D carbon materials through covalent coupling of terminal alkyne on Ag foil, another arylalkyne compound, 1,3,5-triethynylbenzene (TEB) was selected as precursor. The resulted TEB-derived carbon film may exhibit different extraordinary properties in electronics, optics, and mechanics from graphdiyne. And with larger van der Waals pores defined by the framework, TEB-derived film might have different applications, such as gas purification and energy storage in the area that graphdiyne could not satisfy.

The experimental setup of the CVD system is depicted in Figure S9 in the Supporting Information. A silver-foil enclosure was also used and TEB powder was put in a quartz bottle with two tiny holes to decrease the sublimation rate of TEB which is beneficial for attaining an ordered structure. The precursor was sublimated upstream by heating with a heating belt and transported by carrier gas onto the Ag surface. The schematic view of the growth process is similar, and the schematic view is also shown in Figure S9 in the Supporting Information. Details on the growth procedure are presented in Supporting Information. The film also could be transferred from growth substrate onto arbitrary substrates, and the thickness appeared uniform when inspected by OM on SiO_2/Si (**Figure 4**a). The AFM image shown in Figure 4b reveals a flat surface and the height profile inset exhibits a similar height of 0.6 nm. Spectroscopic measurements, Raman spectrum, and UV–vis absorption spectrum were also used to inspect the conversion of TEB to the corresponding linked film. Similarly, we did not obtain any signals from the alkynyl group on the single layer film (Figure 4c) until we overlaid the film layer by layer for ten times on a silver substrate. The Raman peak corresponding to the conjugated diyne links in TEB-derived film[37] was obviously observed (Figure S10, Supporting Information). The Raman peak of terminal arylalkynes in TEB monomer centered at 2114 cm^{-1} (Figure S11, Supporting Information) shifted to 2200 cm^{-1} in TEB-derived film after CVD growth. The comparison of UV–vis adsorption spectra of TEB in THF and TEB-derived film transferred on quartz is depicted in Figure 4d. Similarly, the TEB-derived film on quartz possesses a new broad peak at around 330 nm attributed to the increased delocalization of electrons in the extended conjugation of the film.[36] The corresponding optical transmission spectrum is also shown in Figure S12 in the Supporting Information which reveals that the film is almost completely transparent in the UV–vis region. These results suggest that TEB monomers on the Ag surface undergo a homocoupling reaction to form a linked film.

The electronic transport measurements of TEB-derived film were also performed. The *I–V* curve of TEB-derived film is shown in Figure 4e. The measured resistance is 7.7 MΩ with the corresponding conductivity of 0.27 S cm^{-1}. Figure 4f is the

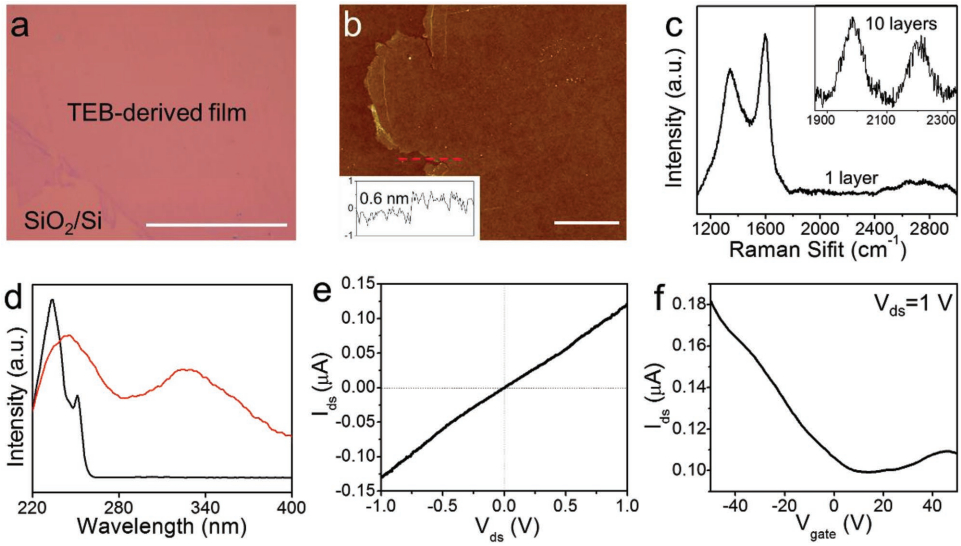

Figure 4. Morphological, spectroscopic, and electrical characterization of TEB-derived film. a) OM image of TEB-derived film transferred on SiO_2/Si. b) AFM image of the film transferred on SiO_2/Si. Inset shows the height profile along the dashed red line. c) Raman spectrum of TEB-derived film transferred on SiO_2/Si. Inset: Raman spectrum of 10-layer transferred TEB-derived films on silver substrate. d) Absorption spectra of TEB in THF (black line) and transferred film (red line) on quartz. e) *I–V* characteristic of TEB-derived film. f) Transport characteristic curve of the film at V_{ds} = 1 V. Scale bars: 50 μm in (a) and 1 μm in (b).

transfer characteristics of TEB-derived film, which displays a p-type semiconducting feature. The electrical conductivity of TEB-derived film is a little worse compared with the film grown with HEB, as TEB-derived film has lower conjugation extent.

In addition, to investigate the effect of different substrates, we performed a CVD growth process with HEB as precursor on Cu surface. The OM image of the as-grown film is shown in Figure S13 in the Supporting Information. From *I–V* characteristics (Figure S14, Supporting Information) we observed that the electrical resistance of the film grown on the Cu surface is much larger than on the Ag surface, suggesting poor quality of the film. Previous work already found that the surface-assisted homocoupling reaction of arylalkynes was not efficient on the Cu substrate as observed by UHV scanning tunneling microscopy.[26] In addition, as the balance between molecule–substrate interaction and intermolecular coupling is a key factor to control the structure of the material, the surface on which the precursor has high surface mobility and relatively low coupling affinity is suitable for growth of regular structures. With the mobility of molecules being reduced on the Cu surface due to strong interaction between molecule and the surface, the formation of extended and regular networks on the Cu surface is significantly blocked. Our results provide the evidence that the silver surface is better than the copper surface.

Extended π-conjugation systems such as graphene[38,39] always have the potential to suppress fluorescence and enhance Raman signals of adsorbed molecules. To investigate the ability of suppressing fluorescence and enhancing Raman signals, we compared the Raman spectrum of four probe molecules (rhodamine 6G (R6G), copper phthalocyanine (CuPc), protoporphyrin IX (PPP), and crystal violet (CV)) on the film grown with HEB and on SiO_2/Si substrate, respectively. The chemical structures of these molecules are shown in Figure S15 in the Supporting Information. These molecules were deposited equally on the carbon film and SiO_2/Si substrate by solution soaking or vacuum evaporation.

Figure 5a is the schematic illustration of the molecules on two substrates and measurement procedure. The black line in Figure 5b is a typical Raman-fluorescence spectrum of R6G molecules on SiO_2/Si substrate at 514 nm excitation. Only a strong fluorescence background was obtained. In contrast, for R6G adsorbed on the as-grown film, the fluorescence emission was weaker and the Raman signals were clearly obtained (red line in Figure 5b). We also observed a similar result on PPP. Assignment of Raman peaks of PPP on the linked film is shown in Figure S16a in the Supporting Information. In addition, when we deposited R6G mixed with HEB molecules on SiO_2/Si substrate, only strong fluorescence background resulting from R6G was observed (Figure 5d). This result suggests that it is not the HEB monomer which contains phenyl and alkynyl group suppress fluorescence, but the linked film. For further investigating Raman enhancement properties of as-grown film, we used CuPc and CV molecules as Raman probes. The Raman signals of CuPc (Figure 5c) and CV (Figure S16b, Supporting Information) on the as-grown film are much stronger than those on SiO_2/Si substrates at 514 nm excitation. The assignments of these Raman peaks are in accordance with previous reports. Moreover, we also found that the TEB-derived film showed similar properties of suppressing fluorescence and enhancing Raman signals of adsorbed molecules (Figure S17, Supporting Information). But on the film grown on Cu foil with HEB, we did not observe such results (Figure S18, Supporting Information).

The exact origin of this phenomenon is not very clear yet. As conjecture, we contribute this phenomenon to chemical enhancement due to the much easier charge transfer between the linked carbon film and molecules. Figure S19 in the Supporting Information shows the comparisons of Raman signals

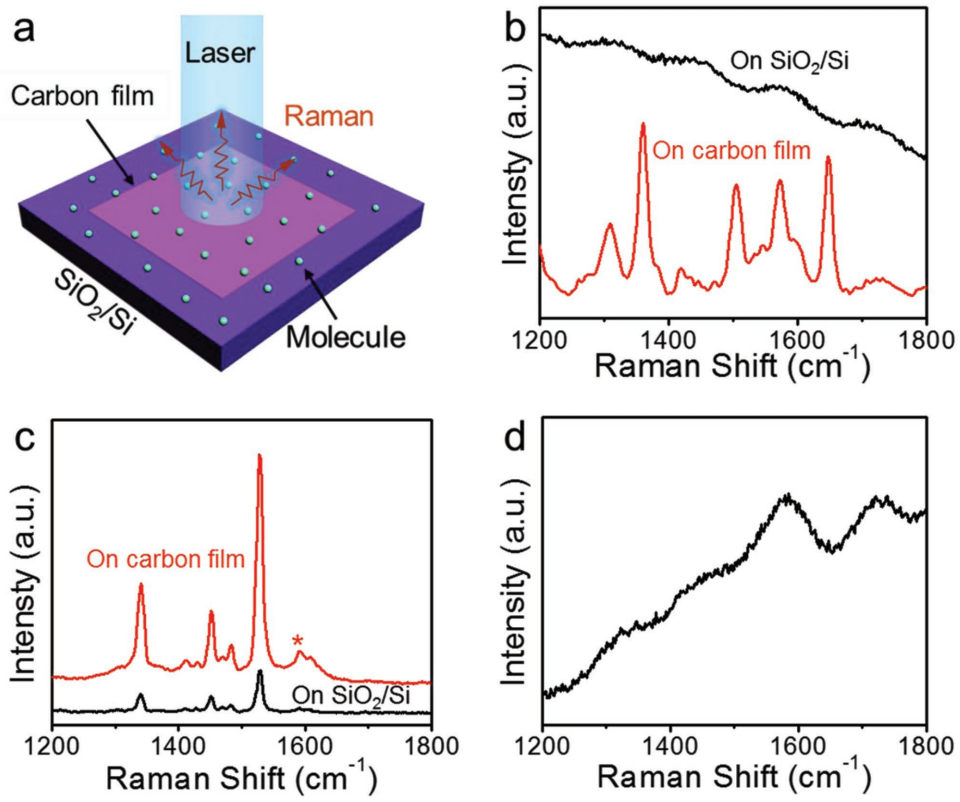

Figure 5. Raman enhancement effect on linked carbon film. a) Schematic illustration of the molecules on substrates and measurement procedure. Comparisons of Raman signals of b) R6G and c) CuPc deposited on the as-grown film (red line) and on SiO_2/Si substrate (black line) at 514 nm excitation. The peak marked by the star (*) is the Raman signal corresponding to the carbon film. d) Raman spectrum of R6G mixed with HEB molecule.

of CuPc deposited on linked carbon films and SiO_2/Si substrate in a larger range. And Table S1 in the Supporting Information listed the corresponding spectral parameters obtained by fitting the peaks with Lorentzian line shapes. The Raman enhancement factors are calculated by comparing the intensity of the Raman signals of CuPc on the as-grown film with that on the blank SiO_2/Si substrate. The enhancement factors for different vibrational modes are obviously different. It is believed that the enhancement factors that varied over a range is due to the selection rules of the chemical enhancement effect.[39] The magnitude of the enhancement, two to five times and the vibration dependence of the enhancement factors are both consistent with the chemical enhancement mechanism. In addition, we also observe an obvious difference in the Raman shift of the vibrational modes of the CuPc molecule on an as-grown film relative to that on the SiO_2/Si substrate. The shift of the Raman peaks indicates the charge-transfer interaction between the CuPc molecule and the linked carbon film. Therefore, we conjecture that enhancement of the Raman signals on the as-grown film is due to the charge-transfer interaction between the as-grown film and CuPc.

In summary, we have introduced a CVD synthesis method for the growth of a linked carbon monolayer with acetylenic scaffoldings by using HEB as precursor, which provides a possible way for fabricating graphdiyne. The covalent coupling reaction of terminal alkynes on a silver surface was demonstrated by spectroscopic analysis. The extended π-conjugation system provided the linked film with the superior electrical conductivity. Moreover, the film showed potential as a substrate for suppressing fluorescence and enhancing Raman signals of adsorbed molecules. By simply replacing HEB with TEB as the precursor, a TEB-derived film was successfully grown on silver foil. This method thereby provides a route for the synthesis of other newly structured 2D carbon materials by using molecular building blocks.

Experimental Section

Growth of Linked Carbon Monolayer with HEB: The synthesis of the linked film was performed in an atmospheric pressure chemical vapor deposition system using HEB as precursor and silver foil as substrate. Details on the growth methodology are provided in Supporting Information.

Transfer Method: The as-grown film was transferred by bubbling method.[40] To transfer the film from growth substrate onto the target substrate, the Ag foil with the as-grown film on it was spin coated with PMMA and subsequently baked at 60 °C for 10 min. Then a bubbling transfer method based on a water electrolysis was used. The PMMA/linked carbon layer was detached from the Ag substrate in seconds by H_2 bubbles generated at the interface between the film and Ag substrate. After rinsing in ultrapure water, the floating PMMA/linked carbon layer was picked up by the target substrate. Then PMMA was removed by hot acetone, leaving the linked carbon film on target substrate.

Characterizations: The prepared film was systematically characterized using optical microscopy (Olympus DX51), AFM (Bruker Dimension Icon, peak force tapping), Raman spectroscopy (Horiba, LabRAM HR-800; excitation light, 514 nm), UV–visible spectroscopy (Perkin-Elmer Lambda 950 spectrophotometer), XPS (Kratos Analytical AXIS-Ultra with

monochromatic Al Kα X-ray), and TEM (FEI Tecnai F20; acceleration voltage, 200 kV).

Device Fabrication and Electrical Measurements: A conventional back-gated configuration with degenerately doped silicon wafer as gate and a layer of 300 nm thick silicon dioxide as gate dielectric was used. The as-grown film was first transferred onto SiO_2/Si substrate. Then metal contacts were deposited on it by sequential thermal evaporation of chromium (8 nm) and gold (80 nm) with the aid of shadow mask based on a TEM grid. Square-shaped contact pattern arrays were formed. Channel length and width of the device were 36 and 6 µm, respectively. The electrical measurements were carried out at room temperature in air.

Raman Enhancement Effect on Linked Carbon Film: R6G, PPP, CV, and CuPc were all commercially available and were used directly as received. Two methods were used for molecular deposition: solution soaking and vacuum thermal evaporation. For solution soaking method, the as-grown film on SiO_2/Si was soaked in the solution of related molecules with the concentration of 10×10^{-6} M for 30 min. Then the sample with adsorbed molecules was rinsed with the corresponding solvents and dried under flowing nitrogen. For another method, the molecules were deposited on the substrate by standard thermal evaporation. The base pressure for deposition is about 10^{-4} Pa, and the deposition thickness of the molecules is 2 Å. The Raman measurement was carried out using a Horiba HR800 Raman system with a 514 nm laser. A 100× objective was used to focus and collect Raman signals. The comparisons of Raman spectra were collected under the same conditions.

Supporting Information

Supporting Information is available from the Wiley Online Library or from the author.

Acknowledgements

This work was supported by the Ministry of Science and Technology of China (2016YFA0200101 and 2016YFA0200104) and the National Natural Science Foundation of China (Grants 51432002, 21129001, 21233001).

Received: August 31, 2016
Revised: December 28, 2016
Published online: March 2, 2017

[1] H. W. Kroto, J. R. Heath, S. C. Obrien, R. F. Curl, R. E. Smalley, *Nature* **1985**, *318*, 162.
[2] S. Iijima, *Nature* **1991**, *354*, 56.
[3] K. S. Novoselov, A. K. Geim, S. V. Morozov, D. Jiang, Y. Zhang, S. V. Dubonos, I. V. Grigorieva, A. A. Firsov, *Science* **2004**, *306*, 666.
[4] R. H. Baughman, H. Eckhardt, M. Kertesz, *J. Chem. Phys.* **1987**, *87*, 6687.
[5] M. M. Haley, S. C. Brand, J. J. Pak, *Angew. Chem. Int. Ed.* **1997**, *36*, 836.
[6] A. Bhaskar, R. Guda, M. M. Haley, T. Goodson, *J. Am. Chem. Soc.* **2006**, *128*, 13972.
[7] Y. Yang, X. Xu, *Comput. Mater. Sci.* **2012**, *61*, 83.
[8] L. Sun, P. H. Jiang, H. J. Liu, D. D. Fan, J. H. Liang, J. Wei, L. Cheng, J. Zhang, J. Shi, *Carbon* **2015**, *90*, 255.
[9] N. Narita, S. Nagai, S. Suzuki, K. Nakao, *Phys. Rev. B* **1998**, *58*, 11009.
[10] M. Q. Long, L. Tang, D. Wang, Y. L. Li, Z. G. Shuai, *ACS Nano* **2011**, *5*, 2593.
[11] K. Srinivasu, S. K. Ghosh, *J. Phys. Chem. C* **2012**, *116*, 5951.
[12] S. W. Cranford, M. J. Buehler, *Nanoscale* **2012**, *4*, 4587.
[13] N. L. Yang, Y. Y. Liu, H. Wen, Z. Y. Tang, H. J. Zhao, Y. L. Li, D. Wang, *ACS Nano* **2013**, *7*, 1504.
[14] G. X. Li, Y. L. Li, H. B. Liu, Y. B. Guo, Y. J. Li, D. B. Zhu, *Chem. Commun.* **2010**, *46*, 3256.
[15] G. X. Li, Y. L. Li, X. M. Qian, H. B. Liu, H. W. Lin, N. Chen, Y. J. Li, *J. Phys. Chem. C* **2011**, *115*, 2611.
[16] J. Y. Zhou, X. Gao, R. Liu, Z. Q. Xie, J. Yang, S. Q. Zhang, G. M. Zhang, H. B. Liu, Y. L. Li, J. Zhang, Z. F. Liu, *J. Am. Chem. Soc.* **2015**, *137*, 7596.
[17] C. S. Huang, S. L. Zhang, H. B. Liu, Y. J. Li, G. T. Cui, Y. L. Li, *Nano Energy* **2015**, *11*, 481.
[18] X. Zhang, M. S. Zhu, P. L. Chen, Y. J. Li, H. B. Liu, Y. L. Li, M. H. Liu, *Phys. Chem. Chem. Phys.* **2015**, *17*, 1217.
[19] X. Gao, J. Zhou, R. Du, Z. Xie, S. Deng, R. Liu, Z. Liu, J. Zhang, *Adv. Mater.* **2016**, *28*, 168.
[20] C. Jinming, P. Ruffieux, R. Jaafar, M. Bieri, T. Braun, S. Blankenburg, M. Muoth, A. P. Seitsonen, M. Saleh, F. Xinliang, K. Mullen, R. Fasel, *Nature* **2010**, *466*, 470.
[21] L. Grill, M. Dyer, L. Lafferentz, M. Persson, M. V. Peters, S. Hecht, *Nat. Nanotechnol.* **2007**, *2*, 687.
[22] D. F. Perepichka, F. Rosei, *Science* **2009**, *323*, 216.
[23] Z. Yi-Qi, N. Kepcija, M. Kleinschrodt, K. Diller, S. Fischer, A. C. Papageorgiou, F. Allegretti, J. Bjork, S. Klyatskaya, F. Klappenberger, M. Ruben, J. V. Barth, *Nat. Commun.* **2012**, *3*, 1286.
[24] B. Cirera, Y. Q. Zhang, J. Bjork, S. Klyatskaya, Z. Chen, M. Ruben, J. V. Barth, F. Klappenberger, *Nano Lett.* **2014**, *14*, 1891.
[25] J. Eichhorn, W. M. Heckl, M. Lackinger, *Chem. Commun.* **2013**, *49*, 2900.
[26] H. Y. Gao, J. H. Franke, H. Wagner, D. Y. Zhong, P. A. Held, A. Studer, H. Fuchs, *J. Phys. Chem. C* **2013**, *117*, 18595.
[27] G. Hong-Ying, H. Wagner, Z. Dingyong, J. Franke, A. Studer, H. Fuchs, *Angew. Chem. Int. Ed.* **2013**, *52*, 4024.
[28] M. Bieri, M. T. Nguyen, O. Groning, J. M. Cai, M. Treier, K. Ait-Mansour, P. Ruffieux, C. A. Pignedoli, D. Passerone, M. Kastler, K. Mullen, R. Fasel, *J. Am. Chem. Soc.* **2010**, *132*, 16669.
[29] X. S. Li, C. W. Magnuson, A. Venugopal, R. M. Tromp, J. B. Hannon, E. M. Vogel, L. Colombo, R. S. Ruoff, *J. Am. Chem. Soc.* **2011**, *133*, 2816.
[30] S. S. Chen, H. X. Ji, H. Chou, Q. Y. Li, H. Y. Li, J. W. Suk, R. Piner, L. Liao, W. W. Cai, R. S. Ruoff, *Adv. Mater.* **2013**, *25*, 2062.
[31] M. E. Ayhan, G. Kalita, S. Sharma, M. Tanemura, *Phys. Status Solidi RRL* **2013**, *7*, 1076.
[32] X. Li, W. Cai, J. An, S. Kim, J. Nah, D. Yang, R. Piner, A. Velamakanni, I. Jung, E. Tutuc, S. K. Banerjee, L. Colombo, R. S. Ruoff, *Science* **2009**, *324*, 1312.
[33] B. Cirera, Y. Q. Zhang, S. Klyatskaya, M. Ruben, F. Klappenberger, J. V. Barth, *ChemCatChem* **2013**, *5*, 3281.
[34] C. Fang, A. V. Ellis, N. H. Voelcker, *J. Electroanal. Chem.* **2011**, *659*, 151.
[35] R. Pérez, A. Rupérez, J. J. Laserna, *Anal. Chim. Acta* **1998**, *376*, 255.
[36] M. J. Schultz, X. Y. Zhang, S. Unarunotai, D. Y. Khang, Q. Cao, C. J. Wang, C. H. Lei, S. MacLaren, J. Soares, I. Petrov, J. S. Moore, J. A. Rogers, *Proc. Natl. Acad. Sci. USA* **2008**, *105*, 7353.
[37] J. Y. Wang, S. Q. Zhang, J. Y. Zhou, R. Liu, R. Du, H. Xu, Z. F. Liu, J. Zhang, Z. R. Liu, *Phys. Chem. Chem. Phys.* **2014**, *16*, 11303.
[38] L. M. Xie, X. Ling, Y. Fang, J. Zhang, Z. F. Liu, *J. Am. Chem. Soc.* **2009**, *131*, 9890.
[39] X. Ling, L. M. Xie, Y. Fang, H. Xu, H. L. Zhang, J. Kong, M. S. Dresselhaus, J. Zhang, Z. F. Liu, *Nano Lett.* **2010**, *10*, 553.
[40] L. B. Gao, W. C. Ren, H. L. Xu, L. Jin, Z. X. Wang, T. Ma, L. P. Ma, Z. Y. Zhang, Q. Fu, L. M. Peng, X. H. Bao, H. M. Cheng, *Nat. Commun.* **2012**, *3*, 7.